Kufa Journal of Engineering
Vol. 11, No. 4, October 2020, P.P. 58-71
Received 5 June 2020, accepted 15 July 2020

NUMERICAL SIMULATION OF NATURAL CONVECTION FOR RAISED-CEILING ROOFTOP HEATED FROM BELOW

Ola Kamiyo[1]

[1] **Senior Lecturer in Heat Transfer and Air conditioning, Department of Mechanical Engineering, University of Lagos, Lagos, Nigeria. Email: *okamiyo@unilag.edu.ng***

http://dx.doi.org/10.30572/2018/kje/110405

ABSTRACT

Attic design has a significant impact on buildings' energy performance thus making investigation of its thermal performance characteristics imperative. Raised-ceiling is among the common complex attic configuration found in pitched-roof buildings. In this study, natural convection inside a raised-ceiling rooftop heated isothermally from the base wall (ceiling) is numerically investigated at a certain pitch angle range while keeping the enclosure base-length unchanged. The results show that the roof pitch and the kinks on the ceiling have a strong influence on the heat and fluid flow patterns. At low roof pitch, high heat transfer rate between the cold and hot walls leads to a multi-cellular flow structure. The number, size and strength of the counter-rotating cells change with the pitch angle. The kinks caused air velocity to double for every 15° increase in the roof pitch. The rate of convective heat transfer is enhanced with decreasing value of the aspect ratio.

KEYWORDS: Raised-ceiling, Rooftop, Pitch angle, Natural convection, Thermal characteristics.

1. INTRODUCTION

The study of thermal performance characteristics in enclosed surfaces is very important due to its wide application in engineering fields such as solar energy systems, cooling of electronic circuits, air conditioning, heat exchangers, roof designs, and many others. With the development of numerical methods, many of the problems of natural convective heat transfer in enclosures could now be accurately analyzed. A review of past studies shows that the flow fields and heat transfer mechanism in the attic of rooftops has received considerable attention by several investigations. With the foundational works of Flack (1980) and Akinsete and Coleman (1982) on the experiment and simulation of rooftop models respectively, many more investigations on pitched roofs in form of triangular enclosures have been considered. Kamiyo *et al*. (2010) and Das *et al.* (2017) carried out comprehensive reviews on regular pitched roofs and some complex-shaped roofs where effects of fluid, heat and geometry properties on various flow regimes and roof configurations are discussed.

More recently, Amrani *et al.* (2017) investigated numerically natural convection with surface radiation heat transfer in a gable roof with eaves in hot climates. Moftakhari *et al.* (2017) used natural element method to study convective and radiative heat transfer analysis of fluid flow inside a triangular cavity. Michels *et al.* (2018) performed computer simulations and experimental measurements in a trapezoidal roof to check the suitability of a test rig to provide results that well-matched a real situation. Difference of 5.6% and 34.3% was obtained for the upward and downward directions of heat flow, respectively. Zhao *et al.* (2019) studied roof-integrated, radiative air-cooling system for energy-saving buildings to reduce the attic temperature of a building. The performance of the radiative air-cooling system was compared with that of shingle roof, attic ventilation, and cool roof to get highest improvement of 18.8%, 41.4%, and 76.1% respectively. Partition displacement effect, flow field and natural convective heat transfer in a trapezoidal cavity having a flexible partition is studied by Mehryan *et al.* (2020) using Arbitrary Lagrangian–Eulerian finite element method. Heat transfer rate in a 30° trapezoidal cavity was found to be 15% lower than that in a square cavity. Many other have been studied but there are still some common ones that investigations have not covered. From the aforementioned literature, most of the previous studies were carried out on conventional, symmetrical pitched roofs and a few complex roof shapes. However, there are some other attic shapes that are not well covered. The raised-ceiling attic configuration in Fig. 1 is one of such shapes and that justifies the present study. This work will be useful to rural farmers in developing countries and building designers in their choice and installation of insulation materials for controlling heat losses into raised-ceiling attic spaces.

Fig. 1. Raised ceiling apartment.

2. METHODOLOGY

The geometry of the raised-ceiling attic investigated in this study is as shown in Fig. 2. The ceiling is raised at angle of half the roof pitch up to one-quarter of the length of the ceiling on both sides making the horizontal part half of the whole ceiling length. This unconventional shape of the ceiling is presumed to influence the flow field and heat distribution within the attic. The enclosure is filled with a viscous, incompressible, Newtonian fluid (air). There is no internal generation of heat. The flow is steady and Bousinessq model applies. Since the real roof size varies, depending on the dimensions of the building, the computational domain dimensions are normalized. The dimensionless form of the governing equations is expressed in the form:

$$\frac{\partial U}{\partial X} + \frac{\partial V}{\partial Y} = 0 \tag{1}$$

$$U\frac{\partial U}{\partial X} + V\frac{\partial U}{\partial Y} = -\frac{\partial P}{\partial X} + \Pr\left(\frac{\partial^2 U}{\partial X^2} + \frac{\partial^2 U}{\partial Y^2}\right) \tag{2}$$

$$U\frac{\partial V}{\partial X} + V\frac{\partial V}{\partial Y} = -\frac{\partial P}{\partial Y} + \Pr\left(\frac{\partial^2 V}{\partial X^2} + \frac{\partial^2 V}{\partial Y^2}\right) + RaPr\theta \tag{3}$$

$$U\frac{\partial \theta}{\partial X} + V\frac{\partial \theta}{\partial Y} = \left(\frac{\partial^2 \theta}{\partial X^2} + \frac{\partial^2 \theta}{\partial Y^2}\right) \tag{4}$$

using the following non-dimensional variables:

$$X = \frac{x}{H},\ Y = \frac{y}{H},\ U = \frac{uH}{\alpha},\ V = \frac{vH}{\alpha},\ \theta = \frac{T - T_C}{T_H - T_C},\ P = \frac{pH^2}{\rho\alpha^2},\ Pr = \frac{v}{\alpha},\ Ra = \frac{g\beta(T_H - T_C)H^3}{\alpha v}$$

The boundary conditions are:

On the base ceiling wall: U = V = 0; θ = 1;

On the roof inclined walls: U = V = 0; θ = 0.

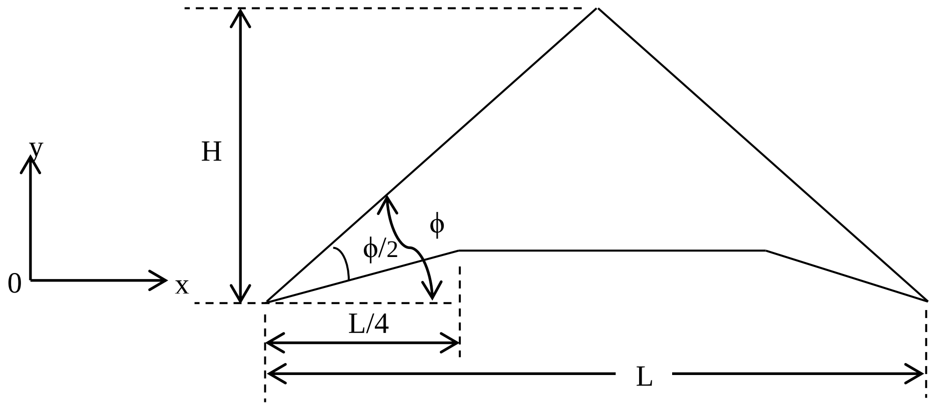

Fig. 2. Physical model.

Four pitch angles within the common range, 14°, 18°, 30° and 45°, representing an aspect ratio range 0.25≤ AR≤ 1.0, were considered and the corresponding Ra values are as stated in Table 1.

Table 1. Parametric details of the enclosures.

Pitch Angle (Φ)	14°	18°	30°	45°
Aspect Ratio, AR	0.25	0.325	0.58	1.00
Rayleigh Number (Ra)	3×10^5	7×10^5	4×10^6	2×10^7

The governing partial differential equations were discretized and solved using a finite volume based CFD code, ANSYS version 18 (2019). Unstructured tetrahedron mesh was used with special attention given to the corners so as to properly resolve the flow situation there. SIMPLE algorithm was employed for the pressure-velocity coupling. The convergence criterion for all the dependent variables is set at 10^{-5}. The grid for the 45° pitch angle is shown in Fig. 3.

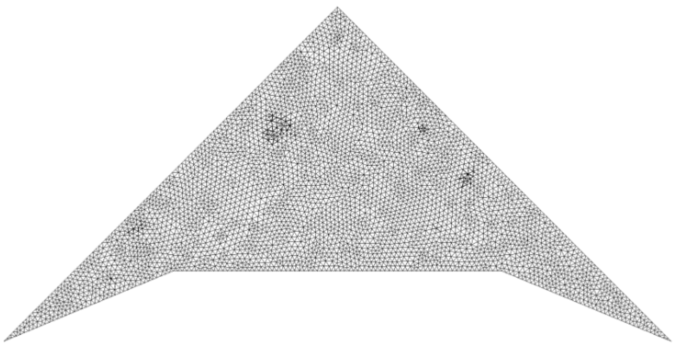

Fig. 3. Computational grid for the 45° pitch angle.

To test the grid independence of the solution scheme, an extensive mesh testing procedure was conducted and the results of the mean Nusselt number variation of some tests are as shown in Table 2. It is concluded that 65,000 elements are sufficient to produce grid independent results.

Table 2. Mean Nusselt number for the grid independence study.

Number of elements	46,806	64,296	73,998
Mean Nusselt number	62.013	53.126	53.552

3. RESULTS AND DISCUSSION

3.1. Flowfield

Results are given in Figs. 4-9 in terms of streamlines and isotherm representations with velocity and Nu plots. Critical observation of the air flow pattern shows that the aspect ratio, AR, which is proportional to the pitch angle, ϕ, has a strong influence on the flow behaviour. At low aspect ratio, the flow hits the upper inclined walls faster and returns; thus, forming recirculating, counter-rotating cells. The number of the cells decreases with increasing pitch angles. The size and strength of the rotating cells also reduce from the midsection towards the bottom corners in a symmetrical pattern. In the 14^0-pitch enclosure, Fig. 4(a), there are fourteen cells formed; the largest cells occupying the midsection rotating with highest intensity. Regions near the intersections of the hot and cold walls are dominated by conduction, hence no fluid movement. In the 14^0 roof pitch, the region extends to about half of the raised sections of the ceiling on both sides.

In Fig. 4(b), the number of vortices has reduced to twelve while still maintaining the symmetrical arrangement. With more headroom, the four cells at the central section in Fig 4(a) seem to have merged to form two large cells with higher rotating strength. The cells reduce in size and intensity towards the kinks. After the kinks, unlike in the 14°-pitch cavity, the higher height of the 18^0-pitch roof created enough space, leading to the formation of a rather elongated cell that limited the conduction region to very near the intersection of the hot and cold walls. The 30° roof pitch, Fig. 4(c), gave a radically different flow structure from other angles. The raised part of the roof frame seems to be losing its strong influence on the flow structure as the kinks could no longer divide the arrangement of the cells, unlike in lower pitch angles. Also, the number of rotating cells has reduced to ten and they have become generally larger. Also, in a manner similar to that observed in Kamiyo *et al* (2014), there are upper rows of cells at the central portion. Fig. 4(d) shows symmetric flow structure with one very large counter-rotating cell at each half of the enclosure, one cell at the kink and one within the raised section of the ceiling. As in other cells, the rotating strength of the central vortex reduces inwardly. However, due to the shape of the enclosure, the multi-cellular flow pattern obtained in this study is different from that observed by Holtzman *et al.* (2000) in their flow visualization experiments performed in an isosceles triangular enclosure heated from the base wall.

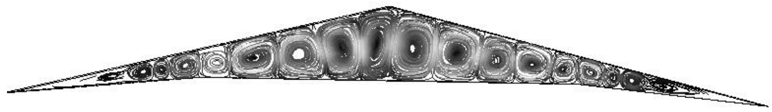

(a) ϕ =14°

(b) ϕ =18°

(c) ϕ =30°

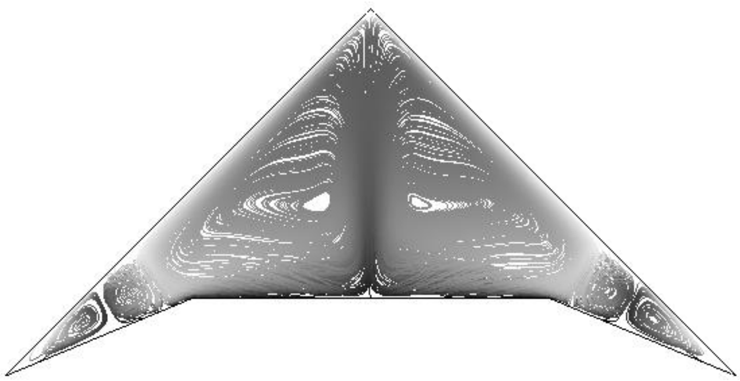

(d) ϕ =45°

Fig. 4. Streamlines for different pitch angles

3.2. Velocity Distribution

The predicted velocity distributions in the attic are shown in Fig. 5 for different pitch angles. The convection currents create a system that show peak values of the flow velocity at the regions where the counter-rotating cells rub each other and reducing towards the center of each cell. Across the cavity, velocity values are relatively high at the midsection but reduce away from it at either side.

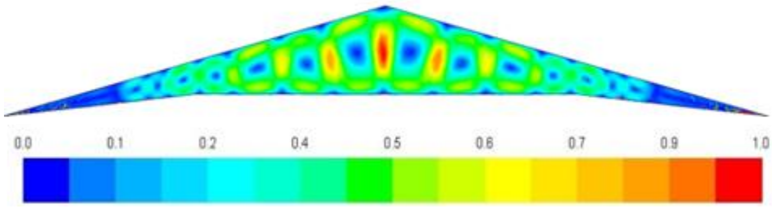

(a) ϕ =14°

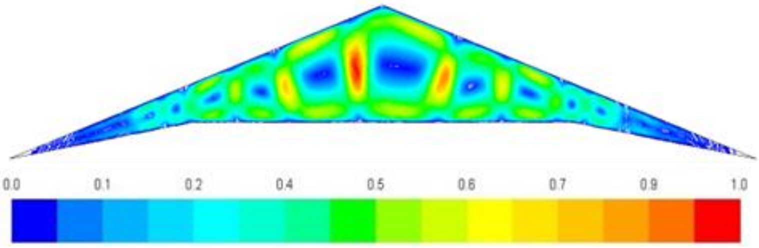

(b) ϕ = 18°

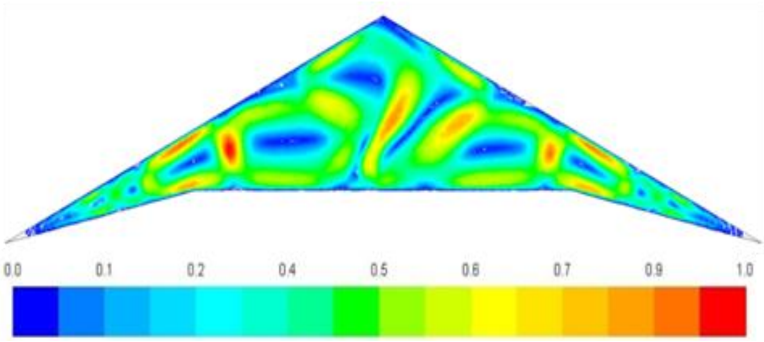

(c) ϕ = 30°

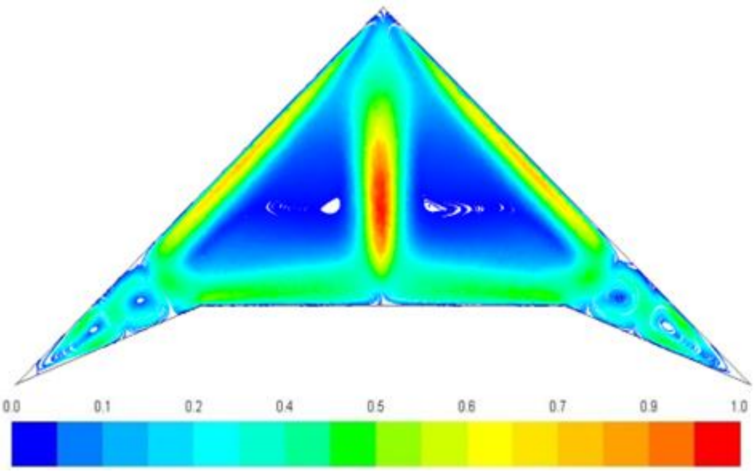

(d) ϕ = 45°

Fig. 5. Velocity contour plots for different pitch angles.

In Fig. 5(a), the high intensity of rotation of the vortices makes the average velocity to be relatively high. For the pitch angles considered, maximum velocity is at the midsection except for the 30°-pitch enclosure. The velocity then reduces on both sides towards the corners with the slowest moving cells immediately after the kinks. In the 18^0-pitch cavity, Fig. 5(b), due to the volume of space and high heat concentration at the midsection, the values of velocity are highest where the largest cell rubs on adjacent cells. In Fig. 5(d), major part of the 45°-pitch cavity is somehow quiescent. To form the large counter-rotating cell, hot air rises from the ceiling at the central portion with relatively high force, hit the apex and splits on either side before flowing down the cold inclined wall with moderate speed while losing the heat content. Large amount of dense cold air moves slowly over the hot ceiling to be heated. After the kinks, due to large space, there is appreciable convection as air circulates at averagely moderate speed.

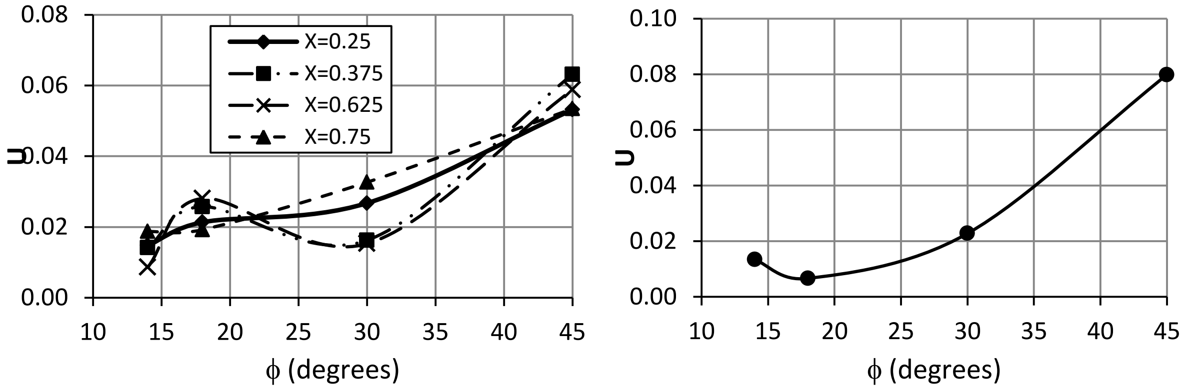

(a) (b)

Fig. 6. Velocity values at Y = 0.5 and (a) at X = 0.25, 0.375, 0.625, 0.75; and (b) at X = 0.5 for each roof pitch.

The plot of values of velocity of air at height Y = 0.5 and at X = 0.25, 0.38, 0.63 and 0.75 for each roof pitch is presented in Fig. 6(a) and at X = 0.5 in Fig. 6(b). The symmetrical flow structure in the enclosures is demonstrated by the near closeness of the plots of the values of the velocity at X = 0.25 and X = 0.75 and the direct overlap of the plots at X = 0.38 and X = 0.63 which are mirror reflection points. In Fig. 6(a), the air velocity value at X = 0.25 in the 45°-pitch cavity is found to be double that at that position in the 30°-pitch cavity which also doubles that at the same position in the 14°-pitch cavity. It can then be concluded that the kink tends to cause the velocity of air in the attic to double for every 15° increase in the roof pitch. Also, it can be seen in Fig. 6(a) that the intensity of the vortices at all points in the 45°-pitch is the highest among the roof pitches considered. In addition, the plot of the air velocity at the mid-centre of the cavities, Fig. 6(b), shows parabolic pattern that indicates quadratic relation between it and the roof pitch.

3.3. Temperature Field

From the temperature contour plots, Fig. 7, the temperature field is characterized by a system of hot air rising along the heated ceiling, splashing onto the cold inclined walls where it loses major part of the convected heat, splitting in either directions and returning in form of cold jets to the ceiling thereby forming convection currents in form of thermal plumes. The plumes occupy regions in-between adjacent thermo-convective recirculating cells as described in Fig. 4. Hence, the number of thermal plumes formed in a cavity is half the number of cells. Also, the larger the cell size and rotating intensity, the thicker the plume formed. For a cavity, the buoyancy force propelling the hot air increases as the Rayleigh number increases leading to increase in the heat transfer rate and formation of more cells as the temperature increases. However, the number of the thermal plumes reduces. This implies that heat transfer rate reduces with increased pitch angle. This is attributed to the hot air rising from the ceiling quickly dissipating its heat content to the cold air that occupies the major part of the attic volume.

In Fig. 7(a) for the 14° roof pitch, the proximity of the cold roof wall and the hot ceiling encourages high rate of heat transfer. The average temperature of the attic is high because the relatively high intensity of rotating cells aid thorough circulation of hot air across the cavity. As the roof pitch increases, the thickness of the boundary layer along the walls increases.

In the 45°-pitch cavity, in Fig. 7(d), the plume at the central portion dissipates its heat content to the low temperature air that occupies that part of the attic space. This makes the central part of the circulating cells averagely isothermal. Also, the return flow of the central cells draws much cold air from the inclined walls such that there appears to be a cutting off of the flow field at the kinks. The cold jets at the kinks almost neutralized the heating effect of the ceiling in the area. It is therefore suggested that insulation thickness around the kinks be increased in order to minimize heat loss into the attic.

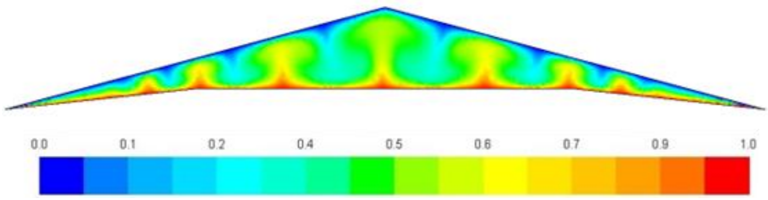

(a) $\phi = 14°$

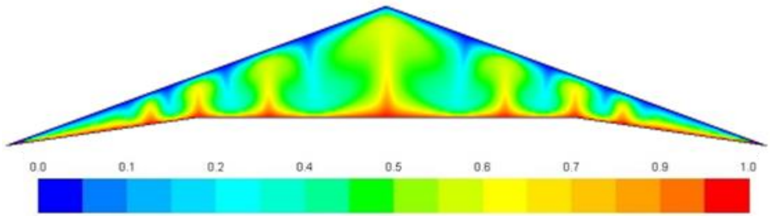

(b) $\phi = 18°$

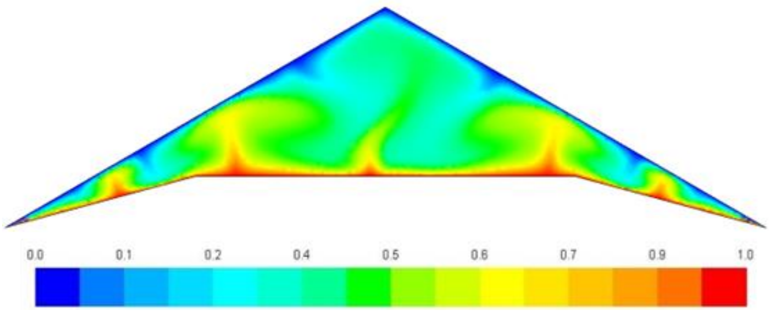

(c) $\phi = 30°$

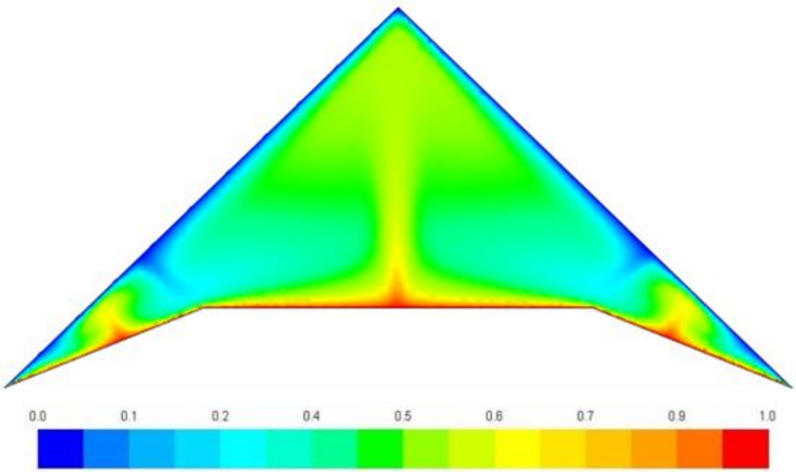

(d) $\phi = 45°$

Fig. 7. Temperature contour plots for different pitch angles.

3.4. Heat Transfer

The heat transfer within the enclosures is understood through the variation of the values of the local heat transfer coefficient along the hot and cold walls expressed in terms of the local Nusselt number defined as:

$$Nu_x = \frac{h_x L}{k} \tag{5}$$

and, the averaged Nusselt number along a wall as:

$$\overline{Nu} = \frac{\bar{h}L}{k} \tag{6}$$

where the ceiling length L, common to the enclosures, is chosen as the characteristic length.

In Fig.8, the variation of the values of the local Nusselt number along the hot and cold walls of the 14°-pitch roof is presented. The sequential sinusoidal pattern of the variation shows that the rate of heat transfer within the cavity links directly with the attaching and detaching processes of the thermal plumes at the hot wall and cold jets at the cold walls. Heat transfer rate goes to lowest value where two counter-rotating cells disconnected air at the same temperature as the ceiling from it thereby creating a region of near-zero temperature gradient at the point. The peak values correspond to points where hot air splashes on the cold inclined roof walls. Near the lower corners, the values of Nu are relatively high due to the proximity of the cold and hot walls, which in turn leads to a high temperature gradient. However, as indicated in Fig.9, the effect of that on the overall thermal efficiency of the system is insignificant.

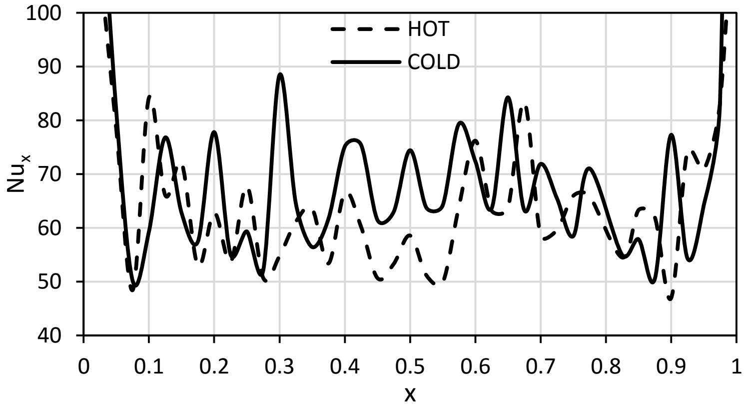

Fig. 8. Local Nusselt number values along the hot and cold walls for 14° pitch angle.

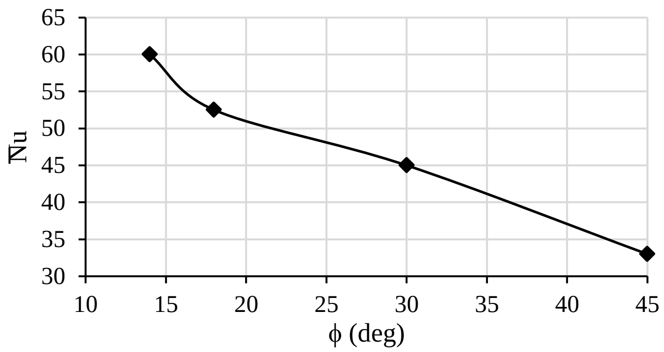

Fig. 9. Average rate of heat transfer from the hot wall for different attic angles.

The variation of the total heat transfer rate in the terms of averaged Nusselt number of the hot ceiling wall with the roof pitch is reported in Fig. 9. The relation is quasi-linear. The thermal power driven by the vortices to the cold walls reduces significantly between 14°- and 45°-pitch angles. Specifically, the value of the mean Nu for the hot ceiling in the 45°-pitch is just about 50% of that in the 14°-pitch. The reason for this is not far-fetched. As the pitch angle increases, the distance between the hot and cold walls increases. Also, the length of the inclined cold wall has increased by 40% more than that of the hot wall and consequently the major part of the cavity becomes colder. As a result, the rate of heat transfer between the walls reduces. The mean Nu value of 33 obtained for the 45°-pitch enclosure with Ra of 2 x 10^7 agrees with the experimental result of Anderson *et al* (2010) where mean Nu value of 35 is obtained for Ra of 5 x 10^7. The practical significance of the results is that when the aim is to minimize heat loss from heated space below the ceiling into the attic, the roof pitch should be made high enough. However, if the focus is drying of agricultural produce as in the rural communities in the developing world, the roof pitch should be made low.

4. CONCLUSION

Thermal characteristics of the attic of a raised-ceiling rooftop heated through the ceiling, depicting the winter condition are numerically investigated at certain pitch angle range while keeping the enclosure base-length unchanged. The results show that the pitch angle and the kinks on the base wall have a strong influence on the heat and fluid flow patterns. At low aspect ratio, the flow hits the upper inclined walls faster and returns; thus, forming recirculating, counter-rotating cells. The number of the cells, however, decreases with increasing pitch angle. The size and strength of the rotating cells also reduce from the midsection towards the bottom corners in a symmetrical pattern. The kinks tend to cause the velocity of air in the attic to double for every 15° increase in the roof pitch. For all pitch-angles, the Nusselt number, Nu is higher at the lower base corners than any part of the flow regime. The rate of convective heat transfer is enhanced with decreasing value of the aspect ratio. The practical significance of the results is that when the aim is to minimize heat loss from heated space below the ceiling into the attic, the roof pitch should be made high enough. However, if the focus is drying of agricultural produce as in the rural communities in the developing world, the roof pitch should be made low.

5. REFERENCES

Akinsete, V.A. and Coleman, T.A. (1982) 'Heat transfer by steady laminar free convection in triangular enclosures', International Journal of Heat Mass Transfer, 25, 991.

Amrani, A. Dihmani, N. Amraqui, S. and Mezrhab, A. (2017) 'Analysis of combined natural convection and thermal radiation heat transfer in a triangular shaped roof for hot climates', Journal of Materials and Environmental Sciences, 8(8), 3013-3027.

Anderson, T.N., Duke, M. and Carson, J.K., (2010) 'Experimental determination of natural convection heat transfer coefficients in an attic shaped enclosure', International Communications in Heat and Mass Transfer, 37(4), 360-363.

ANSYS User's Guide, Release 18, ANSYS Incorporated, (2019).

Das, D. Roy, M. and Basak, T. (2017) 'Studies on natural convection within enclosures of various (non- square) shapes- A review', International Journal of Heat and Mass Transfer, 126, 356-406.

Flack, R. D. (1980) 'The experimental measurement of natural convection heat transfer in triangular enclosures heated or cooled from below', Journal of Heat Transfer, 102, 770-772.

Holtzman, G.A., Hill, R.W. and Ball, K.S., (2000) 'Laminar natural convection in isosceles triangular enclosures heated from below and symmetrically cooled from above', Journal of Heat Transfer, 122(3), 485-491.

Kamiyo, O.M. Angeli, D. Barozzi, G.S. and Collins, M.W. (2014) 'Natural convection in asymmetric triangular enclosures heated from below', Journal of Physics: Conference Series, 547, 1-10.

Kamiyo, O. M. Angeli, D. Barozzi, G. S. Collins, M. W. Olunloyo, V.O.S. and Talabi, S.O. (2010) 'A comprehensive review of natural convection in triangular enclosures', Applied Mechanics Review: Transactions of ASME, 63, 060801, 13 pages.

Mehryan, S.M. Mohammad, G. Reza, K. F. Ahmad, H. and Mohsen, I. (2020) 'Free convection in a trapezoidal enclosure divided by a flexible partition', International Journal of Heat and Mass Transfer, 149, 119186, 14 pages.

Michels, C. Güths, S. Deivis, L. M. and Lamberts, R. (2018) 'Development of an experimental test rig for the evaluation of the thermal performance of building roofs', Energy & Buildings, 180, 32–41.

Moftakhari, A. Aghanajafi, C. Moftakhari, A. and Ghazvin, C. (2017) 'A novel numerical approach for convective and radiative heat transfer analysis of fluid flow problems within triangular cavities using natural element method', Journal of Heat Transfer 139(8), 082002. 13 pages.

Zhao, D. Aili, A. Yin, X. Tan, G. and Yang, R. (2019) 'Roof-integrated radiative air-cooling system', Energy & Buildings, 203, 109453, 9 pages.